Enhanced Simulation of Atmospheric Blocking in a High-Resolution Earth System Model: Projected Changes and Implications for Extreme Weather Events

Yang Gao[1]*, Xiaojie Guo[1,2,3], Jian Lu[4], Tim Woolings[5], Deliang Chen[6,7], Xiuwen Guo[1], Wenbin Kou[1], Shaoqing Zhang[8], L. Ruby Leung[4], Reinhard Schiemann[9], Christopher H. O'Reilly[9], Chuncheng Guo[10,11], Jianping Li[7], Huiwang Gao[1] and Lixin Wu[8]

[1]Frontiers Science Center for Deep Ocean Multispheres and Earth System (FDOMES) and Key Laboratory of Marine Environmental Science and Ecology, Ministry of Education, Ocean University of China, Qingdao, 266100, China
[2]International Center for Climate and Environment Sciences, Institute of Atmospheric Physics, Chinese Academy of Sciences, Beijing, 100029, China
[3]University of Chinese Academy of Sciences, Beijing, 100049, China
[4]Atmospheric, Climate & Earth Sciences Division, Pacific Northwest National Laboratory, Richland, WA, 99354, USA
[5]Atmospheric, Oceanic and Planetary Physics, University of Oxford, OX1 3PU, Oxford, UK
[6]Department of Earth System Science, Tsinghua University, Beijing 100084, China
[7]Department of Earth Sciences, University of Gothenburg, Gothenburg, 40530, Sweden
[8]Frontiers Science Center for Deep Ocean Multispheres and Earth System (FDOMES) and Key Laboratory of Physical Oceanography, Ministry of Education, Ocean University of China, and Laoshan Laboratory, Qingdao, 266100, China
[9]National Centre for Atmospheric Science, University of Reading, Reading, RG6 6ET, UK
[10]NORCE Norwegian Research Centre, Bjerknes Centre for Climate Research, Bergen, Norway
[11]National Centre for Climate Research, Danish Meteorological Institute, Copenhagen, Denmark

*Correspondence to: yanggao@ouc.edu.cn

Key points

1. A high-resolution Earth System Model enhances the simulation of atmospheric blocking frequency in both historical winters and summers.

2. Winter blocking is projected to decrease across the Northern Hemisphere, a trend consistent across both high- and low-resolution models.

3. The high-resolution model projects more frequent and persistent summer blocking, with a shift in location towards central Eurasia.

Abstract

Atmospheric blocking is closely linked to the occurrence of extreme weather events. However, low-resolution Earth system models often underestimate the frequency of blocking, undermining confidence in future projections. In this study, we use the high-resolution Community Earth System Model (CESM-HR; 25 km atmosphere and 10 km ocean) to show that CESM-HR reduces biases in atmospheric blocking for both winter and summer, particularly for events lasting longer than 10 days. This improvement is partly due to reduced sea surface temperature biases at higher resolution. Additionally, applying a bias correction to the 500 hPa geopotential height further enhances blocking frequency simulations, highlighting the crucial role of the mean state. Under the Representative Concentration Pathway 8.5 scenario, CESM-HR projects a decrease in wintertime blocking over regions such as the Euro-Atlantic and Chukchi-Alaska, consistent with previous studies. In contrast, summer blocking is expected to become more frequent and persistent, driven by weakened zonal winds. The blocking center shifts from historical locations over Scandinavia and eastern Russia to central Eurasia, significantly increasing blocking over the Ural region. Summer blocking frequency over the Scandinavia-Ural region may eventually surpass historical winter blocking over the Euro-Atlantic. This increase in summer blocking could exacerbate summer heatwaves in a warming climate, making severe heatwaves, like those observed recently, more common in the future.

Key words: Atmospheric blocking, high-resolution Earth System Model, extreme weather events, Scandinavia–Ural, climate change

Plain Language Summary

Extreme weather events are often linked to atmospheric blocking, a pattern that causes persistent weather conditions lasting days or even weeks. Conventional low-resolution models have struggled to accurately estimate the frequency of atmospheric blocking, undermining confidence in their projections of future weather patterns. Using a more advanced high-resolution model, our study demonstrates a significant reduction in biases of atmospheric blocking during both winter and summer, particularly for long-lasting events. This improvement is partly due to more accurate estimations of sea surface temperatures. Projections under a warming climate suggest a general decline in winter blocking across regions traditionally prone to such events, including the Euro-Atlantic and Chukchi-Alaska areas. In contrast, summer blocking is expected to intensify in both frequency and duration, driven by weakened zonal winds. The center of summer blocking is projected to shift toward central Eurasia, leading to a significant increase in blocking over the Ural region. This rise could exacerbate the intensity of summer heatwaves in the region and downstream areas, implying that severe heatwaves may become more common in the future.

1. Introduction

Atmospheric blocking is an extra-tropical weather system characterized by its persistence, quasi-stationarity, and large spatial scales, significantly affecting local and regional climates by slowing down or obstructing zonal westerly winds (Rex, 1950a, 1950b; Woollings et al., 2018). In the Northern Hemisphere (NH), blocking typically occurs over broad regions, such as the North Atlantic-Europe and North Pacific areas (Pelly & Hoskins, 2003; Schwierz et al., 2004), with more frequent events generally occurring in winter than in summer (Barriopedro et al., 2006).

Blocking has played a crucial role in shaping many recent influential climatic events in the NH (Kautz et al., 2022; Woollings et al., 2018). For example, the series of cold air outbreaks over Europe in the winter of 2010 resulted from the persistent North Atlantic atmospheric blocking (Cattiaux et al., 2010), while extreme cold air outbreaks over North America and Eurasia in 2022 were driven by Alaska blocking and subsequent Ural blocking through Rossby wave propagation (Yao et al., 2023). Similarly, the Russian heatwaves in 2010, responsible for approximately 55,000 deaths (Barriopedro et al., 2011), were primarily attributed to a long-lasting blocking high over western Russia that persisted for over six weeks (Schneidereit et al., 2012). More recently, the 2021 heatwave over the Pacific Northwest, which led to over 1,000 deaths, was triggered by a persistent jet meander and upper-level blocking, seeded and strengthened by latent heat released during an upstream cyclone (Neal et al., 2022). In addition to temperature extremes, blocking is closely linked to hydrological extremes such as heavy precipitation and drought (Dong et al., 2018; Lau & Kim, 2012), wind extremes (Pfahl, 2014), and changes in air quality including surface ozone and particulate pollution (Garrido-Perez et al., 2018; Maddison et al., 2021; Sun et al., 2019). Blocking also influences ocean heat content distribution through its dynamic interactions with synoptic cyclones. Blocking patterns shape the position and trajectory of cyclones, which, in turn, can amplify and sustain blocking via diabatic processes (Steinfeld & Pfahl, 2019; Suitters et al., 2023), regulating northward heat transport into

the Barents Sea (Heukamp et al., 2023).

Simulating the evolution of blocking, along with its frequency and persistence, has long been a challenge. Climate models traditionally underestimate blocking frequencies, particularly over the Euro–Atlantic region, where blocking events are most frequent, especially in winter (Davini & D'Andrea, 2020; Masato et al., 2013; Woollings et al., 2018). This underestimation is primarily due to model limitations and the complexity of blocking mechanisms (Schiemann et al., 2020; Woollings et al., 2018). One effective way to enhance model performance in reproducing the onset and maintenance of blocking is to increase the atmospheric horizontal resolution (Matsueda, 2009; Woollings et al., 2018), which allows for a more accurate representation of small-scale eddies (Anstey et al., 2013), the sharpness of orography (Berckmans et al., 2013), and the fine-scale SST forcing that facilitates more accurate diabatic and convective processes (Schemm et al., 2022; Small et al., 2014).

Through comparisons of four different grid spacings (180, 120, 60, and 20 km) in global atmospheric simulations driven by prescribed sea surface temperature (SST), Matsueda et al. (2009) found that increased horizontal resolution enhanced the ability to reproduce westerly jets and resolve baroclinic eddies, improving the simulation of blocking frequency and maintenance over the Euro–Atlantic region. Using four atmospheric global circulation models, with simulations run at two to three different grid spacings, Schiemann et al. (2017) observed a robust improvement in blocking frequency simulation over the Euro–Atlantic sector in winter with increased horizontal resolution. However, the relationship between summer blocking and model resolution over this region is less clear, and higher resolution did not significantly improve Pacific blocking either (Schiemann et al., 2017). More recently, Jiang et al. (2019) conducted atmospheric simulations using the Energy Exascale Earth System Model at two horizontal resolutions (~25 and ~100 km) driven by prescribed SST. They found little improvement in North Atlantic blocking frequency, although discernible improvements were observed over the North Pacific. Additionally, De Luca et al. (2024) demonstrated

that convective-permitting simulations increased blocking frequency downstream and poleward of the SST front, likely due to improved representation of small-scale processes, highlighting the value of high-resolution models in simulating atmospheric blocking.

The aforementioned numerical experiments, based solely on atmospheric models driven by SST forcing, fail to capture air-sea two-way interactions. Davini and D'Andrea (2016) compared blocking simulations from the Atmospheric Model Intercomparison Project (AMIP) and the Coupled Model Intercomparison Project (CMIP) and suggested that dynamically active air-sea interactions, and hence coupled atmosphere-ocean models, are crucial for accurately simulating blocking events. Reductions in SST biases, such as by increasing the horizontal resolution of the ocean model, are also essential for improving blocking simulations. For example, Scaife et al. (2011) showed that higher ocean resolution reduces North Atlantic SST biases, leading to a significant increase in blocking frequency in single-model experiments, and Athanasiadis et al. (2022) found similar results across multiple models. Moreover, Kwon et al. (2020) and Woollings et al. (2014) emphasized the role of ocean resolution in improving air-sea interactions and SST gradients, further supporting its importance in blocking simulations. To better understand the impact of model resolution on blocking and project its response to global warming, a fully coupled Earth system model with high-resolution atmospheric and oceanic components is essential.

Under a warming climate, a general decrease in blocking frequencies is projected for both winter and summer, with some model agreement (Davini & D'Andrea, 2020; Matsueda & Endo, 2017; Matsueda et al., 2009; Woollings et al., 2018). Despite this consistency among models, a recent review (Woollings et al., 2018) highlighted that confidence in future blocking projections remains low due to pervasive underestimates in blocking frequency, emphasizing the need for model development to improve the reliability of future projections. A regional exception is observed in summer Ural blocking, which may increase in both frequency and intensity in the future (Dunn-

Sigouin & Son, 2013; Woollings et al., 2018). This trend has evolved from no signal in CMIP3 to a statistically insignificant increase in CMIP5, and finally to a significant increase in CMIP6 over a limited area within the Ural region (Davini & D'Andrea, 2020). However, confidence in these projections remains low due to limited significance and sensitivity to the choice of blocking index (Woollings et al., 2018).

In this study, we thoroughly evaluate the capability of a fully coupled Earth system model, with high horizontal resolution for both the atmosphere (25 km) and ocean (10 km) components, to reproduce the frequency and persistence of blocking. We compare this with a multi-model ensemble of low-resolution simulations and, after evaluating the model, discuss future changes in blocking frequency and persistence.

2. Data and methods

2.1 Data descriptions

The data used in this study were obtained from the high-resolution Community Earth System Model (CESM-HR), its low-resolution counterpart (CESM-LR), and the CMIP6 archive. The simulations from CESM-HR, the high-resolution configuration of CESM 1.3, spanned the period from 1850 to 2100. They were based on historical forcings from CMIP5 until 2005, followed by the Representative Concentration Pathway (RCP) 8.5 scenario thereafter. In CESM-HR, the atmosphere and land components were configured with a nominal horizontal resolution of 0.25°, while the ocean and sea-ice components had a nominal horizontal resolution of 0.1°. CESM-LR covered the same time period as CESM-HR, but all components were configured with a nominal horizontal resolution of 1°. The historical period in this study spanned 1975–2004, and the future period was defined as 2071–2100.

For CMIP6, 21 models were used for the historical period based on availability at the time of download, and 11 models were used for the future period. Model details are provided in Table 1. The same historical and future periods were applied to the CMIP6 models and CESM-HR/LR. For the future period, the Shared Socioeconomic Pathway

187 (SSP) 5-8.5 scenario in CMIP6 (Eyring et al., 2016) was selected, as it shares
188 comparable forcing with the RCP 8.5 scenario in CESM-HR/LR. When calculating
189 future changes, only 11 of the 21 models were selected to align with the models used
190 for the future period. Most CMIP6 models used in this study had horizontal resolutions
191 of 1° or lower.

192 Table 1. Coupled Model Intercomparison Project Phase 6 models used in this study[a].

Model	Institution	Spatial resolution (lat. × lon. (°))	Data availability[a]
1. ACCESS-CM2	Commonwealth Scientific and Industrial Research Organization (CSIRO), Australian Research Council Centre of Excellence for Climate System Science (ARCCSS), Australia	1.25 × 1.875	H/F
2. AWI-ESM-1-1-LR	Alfred Wegener Institute, Helmholtz Centre for Polar and Marine Research, Germany	1.875 × 1.875	H
3. BCC-CSM2-MR	Beijing Climate Center, China Meteorological Administration	1.125 × 1.125	H/F
4. CESM2-FV2	National Center for Atmospheric Research, USA	1.875 × 2.5	H
5. CESM2-WACCM		0.9 × 1.25	H/F
6. CESM2		0.9 × 1.25	H
7. CMCC-CM2-HR4	Fondazione Centro Euro-Mediterraneo sui Cambiamenti Climatici, Italy	0.9 × 1.25	H
8. CMCC-CM2-SR5		0.9 × 1.25	H/F
9. CMCC-ESM2		0.9 × 1.25	H/F
10. EC-Earth3-AerChem	AEMET, Spain; BSC, Spain; CNR-ISAC, Italy; DMI, Denmark; ENEA, Italy; FMI, Finland; Geomar, Germany; ICHEC, Ireland; ICTP, Italy; IDL, Portugal; IMAU, The Netherlands; IPMA, Portugal; KIT, Karlsruhe, Germany; KNMI, The Netherlands; Lund University, Sweden; Met Eireann, Ireland; NLeSC, The Netherlands; NTNU, Norway; Oxford University, UK; SURFsara, The Netherlands; SMHI, Sweden; Stockholm University, Sweden; Unite ASTR, Belgium; University College Dublin, Ireland; University of Bergen, Norway;	0.7 × 0.7	H
11. EC-Earth3-CC		0.7 × 0.7	H
12. EC-Earth3-Veg-LR		1.125 × 1.125	H/F
13. EC-Earth3		0.7 × 0.7	H

	University of Copenhagen, Denmark; University of Helsinki, Finland; University of Santiago de Compostela, Spain; Uppsala University, Sweden; Utrecht University, The Netherlands; Vrije Universiteit Amsterdam, the Netherlands; Wageningen University, The Netherlands (EC-Earth consortium)		
14. GFDL-ESM4	National Oceanic and Atmospheric Administration, Geophysical Fluid Dynamics Laboratory, US	1 × 1.25	H
15. IPSL-CM6A-LR	Institut Pierre Simon Laplace, France	1.256 × 2.5	H/F
16. MPI-ESM-1-2-HAM	ETH Zurich, Switzerland; Max Planck Institut fur Meteorologie, Germany; Forschungszentrum Julich, Germany; University of Oxford, UK; Finnish Meteorological Institute, Finland; Leibniz Institute for Tropospheric Research, Germany; Center for Climate Systems Modeling (C2SM) at ETH Zurich, Switzerland	1.875 × 1.875	H
17. MPI-ESM1-2-LR		1.875 × 1.875	H/F
18. NESM3	Nanjing University of Information Science and Technology, China	1.875 × 1.875	H/F
19. NorCPM1	NorESM Climate modeling Consortium consisting of CICERO (Center for International Climate and Environmental Research,), MET-Norway (Norwegian Meteorological Institute), NERSC (Nansen Environmental and Remote Sensing, Bergen 5006), NILU (Norwegian Institute for Air Research7), UiB (University of Bergen), UiO (University of, Oslo 0313) and UNI (Uni Research), Norway (NCC)	1.875 × 2.5	H
20. NorESM2-LM		1.875 × 2.5	H/F
21. NorESM2-MM		0.9 × 1.25	H/F

[a]Data availability, expressed as H or H/F, indicates data availability over the historical period only or both historical and future periods, respectively, for 500 hPa geopotential height.

To ensure a robust comparison between models and observations, this study uses

four reanalysis products. These include the European Centre for Medium-Range Weather Forecasts (ECMWF) fifth-generation global atmospheric reanalysis (ERA5; Hersbach et al., 2020) with a grid spacing of 0.25°, and the Japanese 55-year Reanalysis (JRA-55; Kobayashi et al., 2015) with a grid spacing of 1.25°, both covering the period from 1975 to 2004. The other two datasets are the NCEP Climate Forecast System Reanalysis (CFSR; Saha et al., 2010), covering the period from 1979 to 2008 with a horizontal resolution of ~38 km, and the Modern-Era Retrospective Analysis for Research and Applications, version 2 (MERRA2; Gelaro et al., 2017), covering the period from 1980 to 2009, produced by NASA with a horizontal resolution of 0.5° × 0.625°. The differences in time periods arise from variations in the start years of the reanalysis datasets. To maintain consistency with our models, a 30-year period is selected for each reanalysis product. In the evaluation, blocking events from each reanalysis dataset are first derived, and then an average of the four datasets is used. All simulations, including CESM-HR, CESM-LR, and CMIP6, as well as the reanalysis data, are interpolated to 1° for ease of analysis and comparison.

2.2 Blocking identification method

A two-dimensional hybrid blocking index based on the 500 hPa geopotential height (Z500) is adopted in this study to identify and track atmospheric blocking. The following indices are calculated for each longitude, λ, along a range of latitudes, ϕ, from 40° to 75° N:

$$GHGN(\lambda,\phi)=\frac{Z(\lambda,\phi+\Delta)-Z(\lambda,\phi)}{\Delta}<-10, \tag{219}$$

$$GHGS(\lambda,\phi)=\frac{Z(\lambda,\phi)-Z(\lambda,\phi-\Delta)}{\Delta}>0, \tag{220}$$

$$Z_{\text{anomaly}}(\lambda,\phi)=Z(\lambda,\phi)-\bar{Z}(\phi)>0, \tag{221}$$

where, GHGN (GHGS) represents the meridional gradient to the north (south) of 500

hPa geopotential height, Z represents the 500 hPa geopotential height at longitude λ along latitude ϕ, and $\overline{Z}$ is the zonal mean of Z at latitude ϕ; $\Delta = 15°$. A positive daily zonal anomaly of Z ensures that the blocked points are located within a high-pressure system, minimizing the possibility of identifying cut-off lows (Liu et al., 2018).

If the above conditions are satisfied, the grid point is considered locally blocked. A blocking region is identified if the meridional extension of the blocked points exceeds 15°. For each blocking region, the center is defined as the point where the maximum 500 hPa geopotential height (Z500) is located, and the criteria of Masato et al. (2013) are applied to define a blocking event. For any two consecutive days (e.g., day n and day (n + 1)), if the blocking region center identified on day (n + 1) is within a distance of 27° latitude by 36° longitude from the blocking center on day n, the blocking on these two days is considered a single event. Otherwise, day (n + 1) is considered the start of a new event. If multiple blocking region centers are identified on day (n + 1), the center closest to the blocking center on day n is considered part of the same event. For any given day within the same event, the center should not be more than 1.5 times the distance of 27° latitude by 36° longitude relative to the center on the first day of the event. Additionally, only events that persist for at least five days are considered.

2.3 Bias-corrected blocking detection

Given the strong connection between atmospheric blocking and the mean state of the circulation, a bias correction can be applied to Z500 to improve the detection of blocking events (Scaife et al., 2011; Simpson et al., 2020). To assess the impact of the mean bias in Z500 on blocking, Z500 is corrected by subtracting the daily mean bias for each grid point. This method, referred to as 'dc', involves subtracting the mean bias for the corresponding calendar day (i.e., the same day of the year) from the 30-year historical period. This correction is applied to the original Z500 on a daily basis for each grid point.

2.4 Regional classification and error estimation of blocking events

Blocking events are categorized into specific regions based on the locations they occur. An event is defined to belong to a region, if it satisfies one of the following criteria:

(1) The center of the blocking event (defined as the location of maximum Z500) lies within the region on both the first and last days of the event.

(2) The center of the blocking event is within the region on the first (or last), and the longitudinal coverage of the event on the last (or first) day exceeds half of the region's longitudinal extent.

This classification ensures that events are correctly assigned to their respective regions, even when their spatial coverage partially overlaps multiple regions. These events are referred to as regional blocking events. Additionally, seasonal distinctions are made by considering only those events whose first and last days fall entirely within the respective season (December–February for winter and June–August for summer). For these blocking events, the duration of the event is considered to be the number of blocking days from its onset to termination.

To estimate the sampling uncertainty in blocking event frequency distributions, we use bootstrap resampling to calculate the standard error for each persistence category. Unlike grid point-level resampling, this approach focuses on the counts of blocking events. First, blocking events are identified and categorized by their duration. Then, we perform resampling with replacement on these event counts to generate 1,000 bootstrap samples. The variability in event counts across these samples allows us to calculate the standard error for each duration category. The bootstrap method does not make assumptions about the underlying data distribution, making it particularly effective for small datasets. By balancing computational efficiency with accuracy, this approach provides reliable uncertainty estimates for each persistence category.

3. Characteristics of blocking events in the historical period

3.1 Blocking frequency in winter

Fig. 1 shows the mean fraction of blocking days in winter from 1975 to 2004 over the Northern Hemisphere (NH). The results from each of the four reanalysis datasets are presented in the top row of Fig. S1. According to the mean results from the reanalysis data, winter blocking predominantly occurs in the Euro–Atlantic (30° W–45° E) and Chukchi–Alaska (140° E–150° W) regions. Specifically, the average frequency of blocking over the Euro–Atlantic region is 6% (5.4 days) each winter, while in the Chukchi–Alaska region, it approaches 5% (4.2 days). This pattern is reasonably well captured by CESM-HR, although with some underestimation (Fig. 1b). CESM-HR shows a relatively high number of blocking days in both the Euro–Atlantic and Chukchi–Alaska regions, with larger values in the former. In contrast, the low-resolution models, including CESM-LR (Fig. 1c) and CMIP6 (Fig. 1d), simulate more blocking days over Chukchi–Alaska compared to the Euro–Atlantic region. Specifically, CESM-LR overestimates blocking days in Chukchi–Alaska and underestimates them in the Euro–Atlantic region, which is consistent with previous studies (Davini & D'Andrea, 2020; Dunn-Sigouin & Son, 2013; Masato et al., 2013). Therefore, while the blocking frequency in CESM-HR is still lower than in the reanalysis data, the spatial pattern of blocking is more realistic. Additionally, to confirm that the 30-year period is representative of the climatology of blocking, we further examine the 30-year running mean of blocking frequency from 1885 to 2004 (Fig. S2). During this 120-year period, the 30-year mean blocking frequency in both CESM-HR and CESM-LR remains relatively stable, suggesting that a 30-year period is indeed representative.

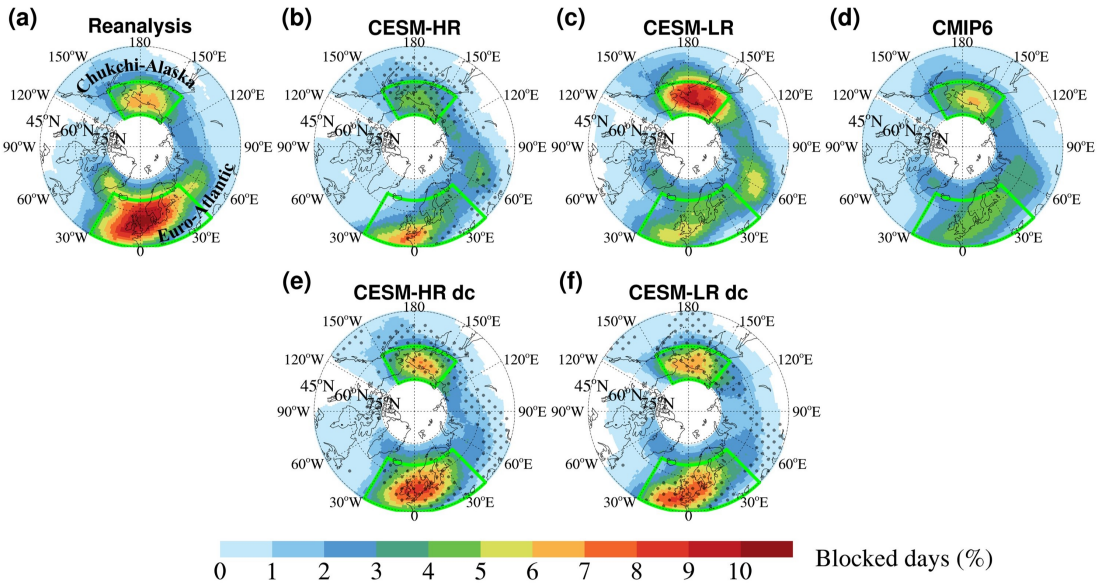

Fig. 1. Mean percentages of atmospheric blocking days in winter during the historical period. (a–d) Results from reanalysis, CESM-HR, CESM-LR, and CMIP6, respectively. (e–f) Results in which the 500 hPa geopotential height (Z500) correction is applied over the simulations at high (CESM-HR) and low (CESM-LR) resolutions. Dots denote areas that show smaller absolute bias than CESM-LR, and the improvement is statistically significant at 95% confidence level based on a two-sided Welch's t-test.

However, CESM-HR does not improve the detection of blockings over the Chukchi-Alaska region. The comparison between CESM-LR and CESM-HR in the two regions suggests that the mechanisms driving blocking biases in the Pacific and Atlantic regions are distinct. The improvement in blocking simulation with an increase in horizontal resolution over the Euro–Atlantic region, but not necessarily over the Pacific, as found in this study, is also reported by Matsueda et al. (2009), who used an atmosphere-only model with four grid spacings (20, 60, 120, and 180 km). These differing sensitivities to distinct maintenance mechanisms between Euro–Atlantic and Pacific blocking could be partly attributed to different dynamical processes. Euro–Atlantic blocking seems to be largely driven by internal atmospheric dynamics, while Pacific blocking is more dependent on oceanic boundary conditions, as suggested by

Tibaldi et al. (1997). However, when comparing different coupled models in CMIP5 with horizontal resolutions ranging from 100 to 500 km, Anstey et al. (2013) found that higher-resolution grid spacings in both atmospheric and oceanic models do not necessarily reduce biases in blocking frequencies, particularly over Greenland and the North Pacific.

Consistently, despite a reduction in mean SST biases over the Pacific region, CESM-HR does not exhibit improved detection of blocking events in the Chukchi–Alaska region. This may indicate that factors beyond mean SST biases, such as SST gradient biases, play a more significant role in simulating Pacific blocking. Specifically, in CESM-HR, high-latitude SST biases do not significantly improve and further overestimate the intensity of the Pacific western boundary currents. In contrast, the improvement over the Euro–Atlantic region when using high-resolution coupled models, consistent with the results from CESM-HR in this study, could be due to increased atmospheric resolution that enhances the simulations of westerly jets and baroclinic eddies (Matsueda et al., 2009). This improvement is also accompanied by a reduced cold bias in the central North Atlantic (Fig. S3a, b), which may enhance diabatic heating and improve blocking formation and maintenance (Athanasiadis et al., 2022; Scaife et al., 2011). This effect could be particularly important over Rossby wave source regions such as the North Atlantic (Li & Sun, 2015; Nie et al., 2019), and it is observed in summer as well (see Section 3.2; Fig. 2 and Fig. S3c).

To further understand the potential causes of spatial heterogeneities between models and reanalysis data, we calculated the anomalies of mean Z500 bias during the historical winter period (Fig. S4d–f), which highlights bias patterns closely associated with atmospheric circulation. CESM-HR exhibits an overestimation of Z500 over the Arctic, reducing the likelihood of meeting the blocking criterion of a positive Z500 gradient between mid-to-high latitudes (e.g., 40°–75° N) and the Arctic, thereby inducing a reduced blocking frequency relative to that observed in reanalysis data. Over the Chukchi–Alaska region in CESM-LR, there is a strong positive Z500 bias,

accompanied by a negative bias on both the northern and southern flanks. This Z500 bias pattern favors identifying more frequent blocking in this area, leading to a positive bias. In contrast, for CESM-HR and CMIP6, the positive bias over the polar area tends to hinder the identification of blocking over Chukchi–Alaska, leading to an underestimation of blocking. Over the Atlantic, the Z500 bias resembles a positive North Atlantic Oscillation (NAO) pattern, which hinders blocking formation over high latitudes. This likely results in an underestimation of blocking in Greenland and a slight southward shift of the blocking center in the Euro–Atlantic region (Woollings et al., 2008). Additionally, this dipolar bias could be linked to regional shifts in wave-breaking activity (Anstey et al., 2013).

To understand how this bias might affect blocking occurrence, we applied a method to correct the Z500 bias on a daily scale, referred to as "dc". The resulting spatial distributions of blocking days (Fig. 1e–f) show substantial improvements across the major blocking areas, including Euro–Atlantic, Chukchi–Alaska, and Greenland, for both CESM-HR and CESM-LR. Moreover, significant improvements in CESM-HR, compared to CESM-LR, are particularly noticeable in the Euro–Atlantic region (Fig. 1e-f). These results further support the notion that blocking biases are closely linked to mean state biases. However, it remains challenging to definitively determine whether the mean state biases in the model directly cause the blocking biases, or if the mean state biases themselves are a reflection of blocking biases. Previous analyses suggest that blocking biases alone cannot explain mean state biases, whereas mean state biases often statistically explain blocking biases (Davini & D'Andrea, 2016; Scaife et al., 2010). Therefore, at least under the conditions of the currently popular blocking indices, blocking biases appear to be more significantly influenced by mean state biases.

3.2 Blocking frequency in summer

Similar to winter, the Euro–Atlantic and Chukchi–Alaska regions remain the primary areas experiencing frequent blocking in summer, although the blocking

distribution shifts toward the center of Eurasia. This pattern is consistent across reanalysis data, CESM-HR, CESM-LR, and CMIP6 (Fig. 2). Specifically, the high-blocking regions extend westward from Chukchi–Alaska to eastern Russia (~120°–180° E) and eastward from the Euro–Atlantic to the Scandinavia–Ural region (~5° W–90° E), with blocking frequencies of 4% (3.9 days per summer) and nearly 4% (3.3 days per summer), respectively, based on the mean result from reanalysis data. The results from each of the four reanalysis datasets are shown in the bottom column of Fig. S1.

When compared to the reanalysis data (Fig. 2a), CESM-HR better captures the spatial distribution of blocking frequency than both CESM-LR and CMIP6. For example, over the Scandinavia–Ural region, CESM-HR shows a significant improvement, with the smallest bias (7%) in total blocking days, in contrast to much larger biases in CESM-LR (−15%) and CMIP6 (−57%). This underestimation has been a long-standing issue with low-resolution models (Davini & D'Andrea, 2020; Scaife et al., 2010). Over eastern Russia, all models show underestimations, though CESM-HR performs slightly better, with a bias of −44%, compared to −56% in CESM-LR and −52% in CMIP6. Improved spatial heterogeneity, particularly the shift of the high-blocking frequency center from the west coast of Europe to the Ural region, has been observed in the 25-km simulations using the Community Atmospheric Model driven by prescribed SST (Schiemann et al., 2017). However, similar to our findings, little improvement is seen over the Pacific sector.

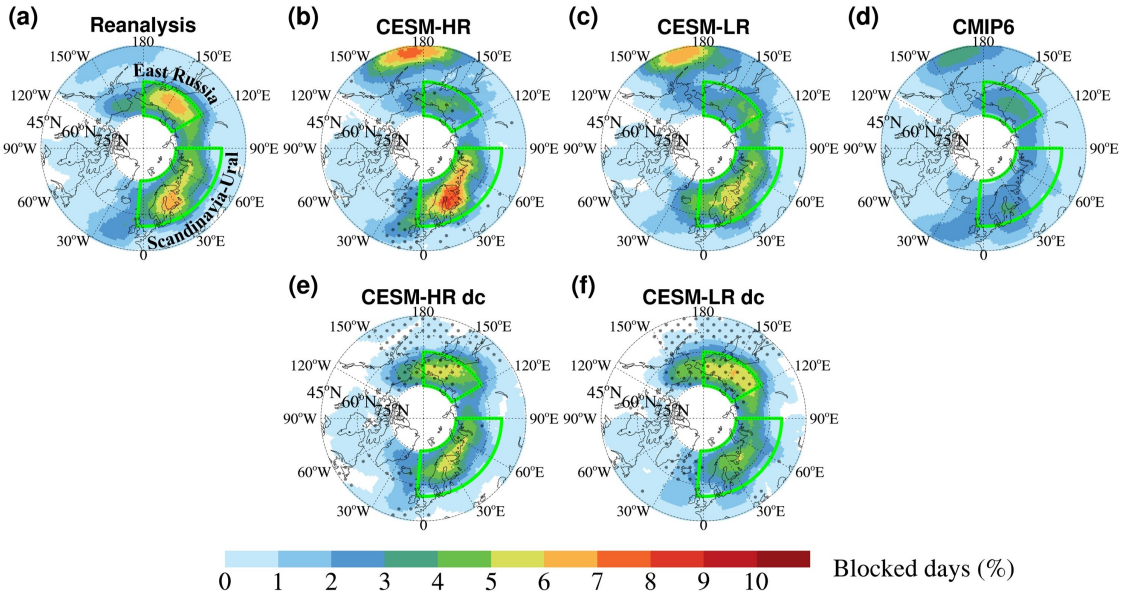

396

397 **Fig. 2. Mean percentages of atmospheric blocking days in summer during the**
398 **historical period.** (a–d) Results from reanalysis, CESM-HR, CESM-LR, and CMIP6,
399 respectively. (e–f) Results in which the 500 hPa geopotential height (Z500) correction
400 is applied over the simulations at high (CESM-HR) and low (CESM-LR) resolutions.
401 Dots denote areas that show smaller absolute bias than CESM-LR, and the
402 improvement is statistically significant at 95% confidence level.

403

404 Similar to winter, daily bias correction is applied to Z500 in summer (Fig. 2e–f).
405 The improvements resulting from Z500 corrections are primarily concentrated in the
406 region from eastern Russia to Alaska. However, these improvements are less
407 pronounced than those observed in winter. One possible explanation is that summer
408 blocking events only weakly satisfy the blocking criteria, meaning that even a small
409 change in Z500 anomalies can significantly influence blocking detection. Furthermore,
410 the bias corrections in CESM-LR seem to hinder blocking detection over the Ural
411 region (Fig. 2f vs. Fig. 2c). A similar effect is seen in CESM-HR, where the corrections
412 effectively reduce the positive bias in this region (Fig. 2e vs. Fig. 2b).

413

414 **3.3 Regional blocking events persistence in winter and summer**

415 The impact of blocking on extreme weather events is closely related to the duration

or persistence of the blocking (Woollings et al., 2018). Blocking creates a stable atmospheric condition, and the longer the blocking persists, the longer weather systems can influence a specific region. For example, the record-breaking 2010 Russian heatwave and the floods in Pakistan were linked to persistent blocking that lasted over six weeks (Schneidereit et al., 2012). Therefore, evaluating models' ability to reproduce blocking persistence is crucial.

Distributions based on the persistence of regional blocking events are shown in Fig. 3. In winter, the reanalysis data indicate a total of 685 days of blocking over the Euro–Atlantic region and 179 days over the Chukchi–Alaska region during the thirty-year winter period. Note that these values may be larger than the product of thirty winter days and fractional blocking days shown in Fig. 1, as the movement of the blocking event means the number of days it affects each grid point can vary. For a given grid point, the number of blocking days is determined by how many days the event covers that specific grid point. However, for regional blocking events, the number of blocking days from the onset to the termination of the event is counted as the duration of the event (see section 2.4), which is likely greater than the maximum occurrence at any single covered grid point.

Consistent with the spatial distributions in Fig. 1, CESM-HR performs better than CESM-LR and CMIP6 in terms of the total number of blocking days. However, CESM-HR underestimates long-lasting regional blocking events in the Chukchi–Alaska region compared to reanalysis data. In the Scandinavia–Ural region, CESM-HR most closely matches the distribution of reanalysis data (represented by the dots in Fig. 3c), although it slightly overestimates the total number of blocking days. CESM-LR performs slightly better in matching the total number of blocking days but does not match the distribution as well as CESM-HR. In contrast, the CMIP6 models underestimate the total number of blocking days by more than half and fail to capture a realistic distribution. Additionally, CESM-HR shows the best distribution over eastern Russia (Fig. 3d).

For long-lived events (i.e., those with persistence > 10 days in both winter and

summer), CESM-HR captures them more accurately in some regions compared to the low-resolution models. For example, in winter over the Euro–Atlantic region, and in summer over the Scandinavia–Ural and Eastern Russia regions, the overall biases for CESM-HR are −12%, −4%, and −69%, respectively. In contrast, CESM-LR and CMIP6 show larger biases: −35% (−48%), −23% (−75%), and −85% (−100%), respectively, for these regions. These improvements align with previous studies (Matsueda et al., 2009), which demonstrated that higher horizontal resolution improves the representation of sub-synoptic-scale eddies, thus enhancing the persistence of regional blocking events. However, in the Chukchi-Alaska region, CESM-HR fails to capture long-lived events effectively, resulting in an underestimation of blocking frequency. This suggests that, while higher resolution improves blocking event representation in many areas, additional factors influencing blocking mechanisms in the Chukchi-Alaska region may not be fully addressed by resolution alone.

Furthermore, the daily-corrected high-resolution simulations (CESM-HR dc, marked with stars in Fig. 3) show improved blocking frequency for short-lived events (5–10 days) across nearly all regions. However, this correction is less effective for long-lived events, except for those over eastern Russia in summer. This suggests that long-lived events are more likely driven by low-frequency variability or remote teleconnections, such as the El Niño–Southern Oscillation (ENSO) (McKenna & Karamperidou, 2023), Arctic sea-ice concentrations (Zhang et al., 2018), and waveguide teleconnection (Xu et al., 2020). The importance of low-frequency processes in the formation and maintenance of summer blocking over Eurasia has been emphasized (Drouard & Woollings, 2018). Additionally, higher ocean resolution may lead to stronger ENSO teleconnections, and the improved simulation of long-duration events in most regions by CESM-HR further enhances confidence in this regard (Williams et al., 2024). Therefore, more attention should be given to the changes in low-frequency processes under global warming and their impact on extreme persistent summer regional blocking events.

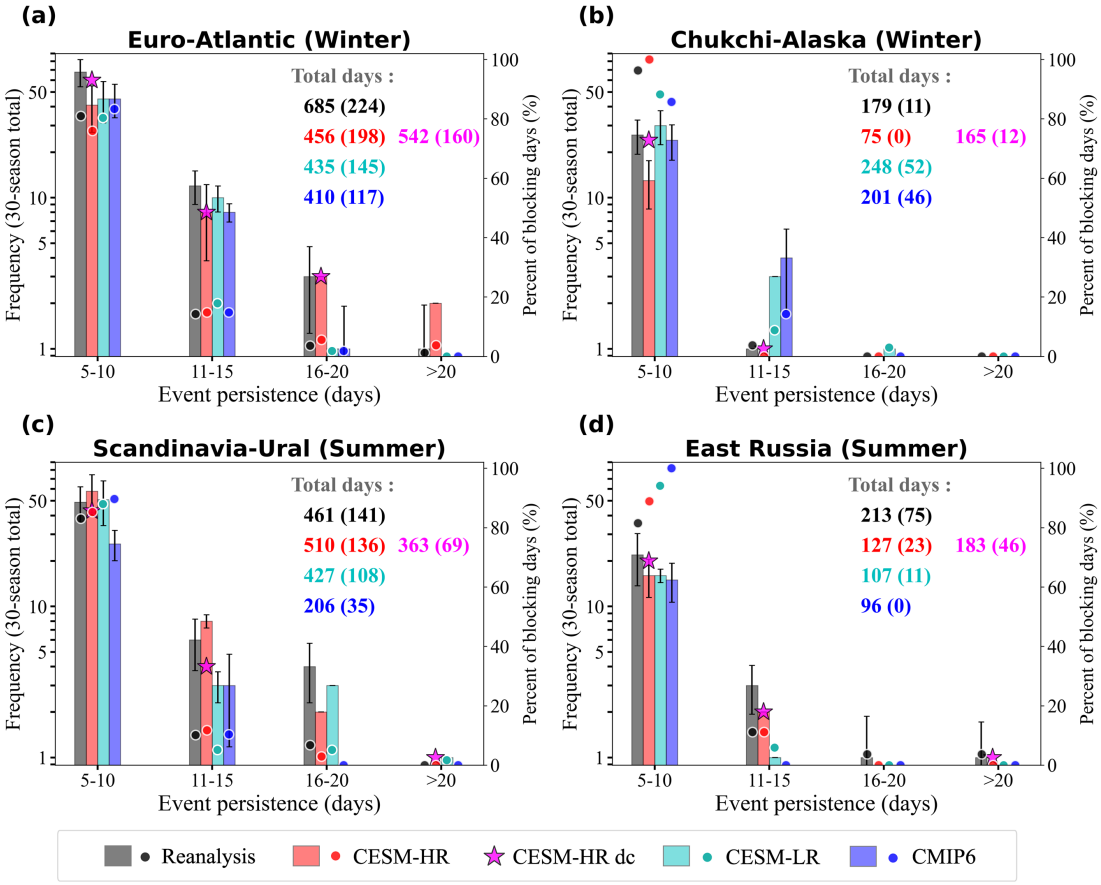

Fig. 3. Seasonal total frequency distributions of regional blocking events in the thirty-year historical period based on persistence. (a, b) represent winter, while (c, d) represent summer; the regions defined as shown in Figs. 1 and 2. The results from reanalysis and CMIP6 represent the averaged results. For CMIP6, durations are filtered before averaging, retaining only those events where the number of models with occurrences exceeds one-third of the total number of models. Stars (magenta) indicate CESM-HR (daily-bias-corrected Z500) results. Dots represent the percentage of events in each persistence bin, corresponding to the right-hand Y axis. The total number of blocking days is shown in each panel with the number in parentheses representing the total number of long-lasting events (>10 days). Error bars represent the standard error of total blocking event durations for each persistence category, estimated using 1,000 bootstrap resampling iterations (see Section 2.4).

4. Future changes in blocking frequency under a warming climate

4.1 Decreases in winter blocking frequency

Projected winter blocking frequencies at the end of this century are shown in Fig. 4. A statistical significance test has been applied to these changes, with both the significance test and model agreement included for the CMIP6 projections. It is important to note that, in future scenarios, the biases used for correction are still derived from the differences between the model and reanalysis data during the historical period. However, assuming a constant bias may not be valid under global warming, as atmospheric circulation responses to warming exhibit distinct seasonal and regional variations (Shaw et al., 2024). Therefore, the daily correction (dc) method should be considered as an additional ensemble member rather than a definitive source suggesting that its projections of future changes are more accurate than those of CESM-HR.

Overall, the future frequencies of blocking (Fig. 4a–d) are spatially consistent with those observed during the historical period, with frequent blocking events occurring in the Euro–Atlantic and Chukchi–Alaska regions. Under the RCP 8.5 scenario, the frequency of blocking tends to decrease across most of the NH, particularly over the Euro-Atlantic region. This pattern is consistent among CESM-HR, CESM-HR dc, CESM-LR, and CMIP6 projections (Fig. 4e–h). A decreasing trend is also evident in the Chukchi–Alaska region, although CESM-HR (dc) projects a slight increase, with weak statistical significance. The projected reductions in winter blocking are consistent with previous studies (Davini & D'Andrea, 2020; Dunn-Sigouin & Son, 2013; Matsueda & Endo, 2017; Matsueda et al., 2009). These changes in blocking are closely tied to alterations in mean wind patterns (de Vries et al., 2013; Dunn-Sigouin & Son, 2013). Future changes in zonal winds at 500 hPa (Fig. S7) indicate that the projected decreases in Euro–Atlantic blocking are spatially linked to enhanced zonal winds.

Given the potential impact of the ENSO on blocking via teleconnection through the Rossby wave train (Barriopedro & Calvo, 2014; Davini & Cagnazzo, 2014; Dunn-Sigouin & Son, 2013; McKenna & Karamperidou, 2023), we further examine how blocking changes are associated with the different phases of the ENSO. According to

CESM-HR, there are a total of 86 El Niño months and 114 La Niña months, which are projected to increase by 13 months and decrease by 3 months, respectively, in the future (see Table S1 for more detailed characteristics of ENSO changes during winter and summer seasons). Changes in blocking frequency are consistent with La Niña conditions, showing an overall decrease (Fig. S8a, c), in contrast to the opposite trend during El Niño phases. These results from CESM-HR are generally supported by CESM-LR (Fig. S8d) and are in line with previous studies (e.g., Dunn-Sigouin and Son (2013)). However, CESM-LR projects a subtle increase in blocking frequency over the Chukchi–Alaska region (Fig. S8b), with no significant change in the sample size for El Niño during the composite analysis (Table S1).

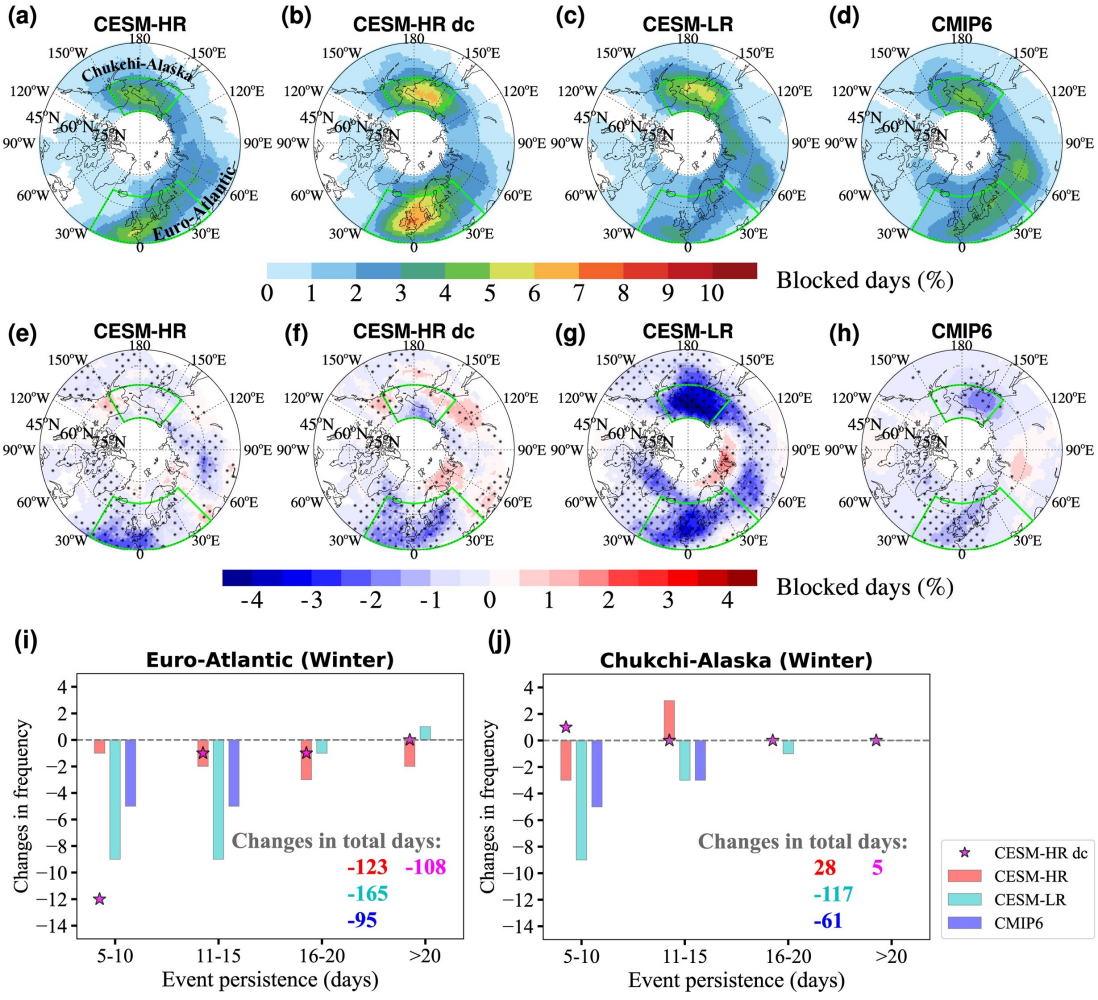

Fig. 4. Winter blocking at the end of this century under representative

concentration pathway 8.5. (a–d) Blocking frequencies in the future. The same correction method using historical bias is applied to the future period of CESM-HR dc. (e–h) Changes in future blocking frequencies relative to the historical period, with dots in panel e-g denoting changes that are statistically significant at 99th level (Welch's t-test). Dots in panel h indicate that at least 70% of CMIP6 models agree with the multi-model mean on the sign of the change, and among these models with agreements, at least 60% show statistically significant changes at 99th level. (i and j), Future changes in blocking frequencies for different regional blocking event persistence values; numbers in the bottom right of each panel indicate changes in total blocking days during a thirty-year winter period. Results are shown at high (CESM-HR) and low (CESM-LR and CMIP6) resolutions, with dc denoting the bias corrections that were applied to daily mean Z500 during both the historical and future periods.

Changes in the persistence of winter regional blocking events are shown in Fig. 4i and j. In the Euro–Atlantic region, all models consistently project decreases in regional blocking events across all persistence categories. Specifically, according to CESM-HR, long-lived events lasting 16–20 days occurred three times, and those lasting longer than 20 days occurred twice, during the historical period (Fig. 3a). However, these long-lived events are projected to disappear in the future (Fig. 4i). Similar decreases are projected for both the Euro–Atlantic and Chukchi–Alaska regions across most persistence categories, though subtle increases are observed in some cases based on CESM-HR. These results are further supported by the CESM-HR findings using the ANM method (Fig. S9).

4.2 Increases in future summer blocking

Projected summer blocking frequencies are shown in Fig. 5a–d. Similar to winter, the spatial distribution of future summer blocking events is consistent with the historical pattern. However, as indicated in Fig. 5e–h, unlike in winter, there is no widespread

decrease in blocking frequency. Notably, CESM-HR (dc) projects a significant increase in summer blocking over central Europe, the Urals, central Siberia, and the Okhotsk region. This increase in summer blocking, combined with a decrease in winter blocking, suggests that summer blocking may become more frequent than winter blocking in the future. Specifically, CESM-HR (dc) indicates a trend toward merging two peak regions: the eastern Russian blocking shifts westward, while the Scandinavian blocking shifts eastward toward the Ural region. In CESM-HR, the largest increase is observed in the Ural region, with CESM-HR dc showing a similar pattern but with an even stronger magnitude. The increases in blocking frequency over Siberia and the Ural region are closely linked to weakened zonal winds (Fig. S7b).

We also examine the influence of the ENSO on blocking frequency. In CESM-HR, El Niño is projected to increase both in frequency and persistence. Specifically, the persistence of El Niño events is projected to increase from an average of 14 months historically to 16.5 months in the future. In contrast, La Niña events are expected to decrease. Composite analysis for the summer season reveals a notable trend: the increase in El Niño and decrease in La Niña contribute to a spatial shift in blocking distribution (Fig. S8e, g). In particular, the increase in summer blocking over the Ural region is partially shaped by La Niña, with a future strengthening of its intensity (−0.08°C). In CESM-LR, while the results are generally consistent with those of CESM-HR (Fig. S8f, h), the enhanced blocking frequency extending from Scandinavia to the Ural region during La Niña events is much weaker, warranting further investigation in future studies. Additionally, previous studies suggest that ENSO teleconnections are expected to strengthen in the future (Beverley et al., 2024; Fereday et al., 2020; Müller & Roeckner, 2008), potentially further influencing the frequency and distribution of regional blocking events. However, caution is needed in interpreting ENSO-induced changes in blocking, as significant uncertainty remains regarding how ENSO will respond to future warming (Alizadeh, 2022; Cai et al., 2021).

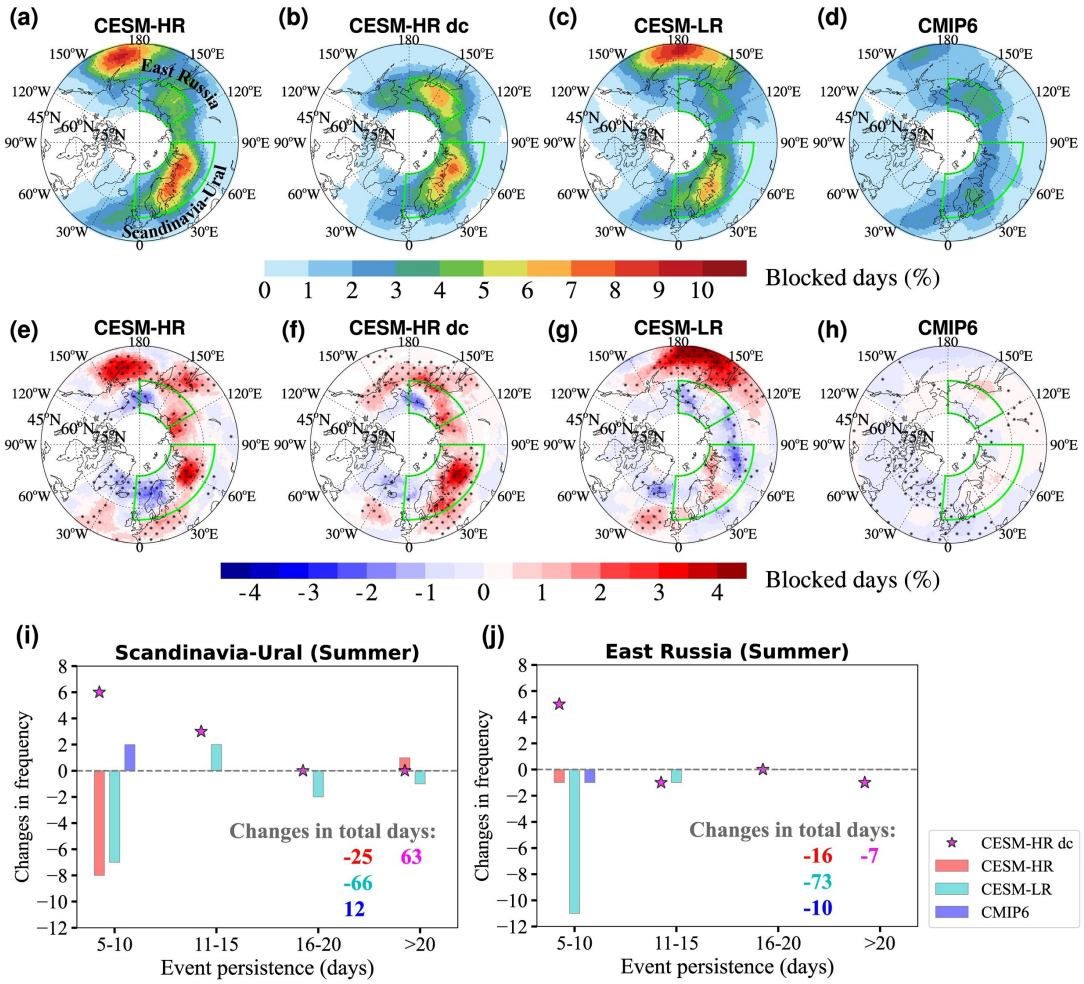

Fig. 5. Summer blocking at the end of this century under representative concentration pathway 8.5. (a–d) Blocking frequencies in the future. (e–h) Changes in future blocking frequencies relative to the historical period, with dots in panel e-g denoting changes that are statistically significant at 99th level (Welch's t-test). Dots in panel h indicate that at least 70% of CMIP6 models agree with the multi-model mean on the sign of the change, and among these models with agreements, at least 60% show statistically significant changes at 99th level. (i and j) Future changes in blocking frequencies for different regional blocking event persistence values; numbers in the bottom-right of each panel indicate changes in total blocking days during a thirty-year summer period.

Previous studies have indicated an overall decrease in summer blocking over mid-to-high latitudes, with the exception of an increase over the Ural region in the future

(Davini & D'Andrea, 2020; Dunn-Sigouin & Son, 2013; Masato et al., 2013; Matsueda & Endo, 2017). CMIP6 models show similar trends, but without statistical significance. Differences in the persistence of summer regional blocking events between the historical and future periods are shown in Fig. 5i and j. In the Scandinavia–Ural region, the models project slightly negative changes in future regional blocking days compared to the historical period. In contrast, CESM-HR shows clear dipolar spatial changes (Fig. 5e). Specifically, for the Scandinavia–Ural region, CESM-HR, which provides the most accurate distribution in this area, does not detect any blocking events with a persistence of over 20 days during the historical period. However, such long-lived events emerge in the future period.

To test the robustness of these high-impact event projections, we conducted 10 random removal experiments for both the historical and future periods. In each experiment, a random subset of blocking days, representing locally blocked grid points, was excluded during the identification of blocking regions, limiting the total number of removed days to 10% of all blocking days (approximately 1,000 days over 30 years). This methodology generated 100 distinct random variations for the future changes, effectively expanding the ensemble size. The results show that 90% of the future scenarios exhibit a transition from no long-lived events to the emergence of such events. Additionally, results from the ANM method further support this increase in blocking events lasting longer than 20 days (Fig. S9).

In eastern Russia, where dipolar spatial changes are projected (Fig. 5e and f), events with shorter durations (5–10 and 11–15 days) tend to show a slight increase according to CESM-HR dc.

Conclusions

This study thoroughly investigates the ability of CESM-HR, its low-resolution counterpart (CESM-LR), and the multi-model ensemble of CMIP6 to simulate blocking

in both winter and summer. During the historical winter period, low-resolution models (e.g., CESM-LR) significantly overestimate blocking frequency in the Chukchi–Alaska region, while underestimating it in the Euro–Atlantic region. In contrast, CESM-HR reduces the underestimation of winter blocking in the Euro–Atlantic, particularly capturing long-lived events lasting over 15 days. During the historical summer period, low-resolution simulations tend to show large underestimations in blocking-prone regions. This bias is substantially reduced in CESM-HR, especially over the Scandinavia–Ural region. A mean bias correction of the 500 hPa geopotential height substantially improves blocking detection in both high- and low-resolution models, suggesting that the primary cause of blocking biases is in the mean state, rather than the representation of synoptic variability. While the mean state accounts for most of the bias, some residual discrepancies remain, particularly over Europe, indicating that the mean state alone cannot fully explain the magnitude of the bias. This suggests that further research is necessary to better understand the blocking mechanism and guide the continued development of climate models.

Looking to the future, winter blocking is projected to broadly decrease across much of the Northern Hemisphere, including the Euro–Atlantic and Chukchi–Alaska regions, primarily due to enhanced westerly winds. This trend is consistent across both high- and low-resolution models. In summer, low-resolution models generally show a weak reduction in blocking, whereas CESM-HR, which provides improved historical simulations, reveals more distinctive patterns. These include a slight decrease in blocking over the Greenland Sea and Chukchi regions, alongside a significant increase in blocking over central Eurasia, particularly in the Ural–northern Siberia region, as a result of weakened westerlies. Historically, winter blocking has occurred much more frequently than summer blocking, and as a result, winter blocking has been more extensively studied, including its characteristics, evolution, and mechanisms. However, the findings here highlight that under a warming climate, future summer blocking may become more frequent than winter blocking. Given the recent increase in heatwaves,

this shift underscores the need for greater attention to summer blocking in future research.

Data availability.

The CESM-HR and LR simulations can be achieved from https://ihesp.github.io/archive/products/ds_archive/Sunway_Runs.html, and the data used in this study will be deposited permanently if the article is eventually accepted. The CMIP6 data is available at https://esgf-data.dkrz.de/search/cmip6-dkrz/ (CMIP6).

Acknowledgements

This work was supported by the National Key Research and Development Program of China (2022YFE0106400), National Natural Science Foundation of China (42122039, 42375189) and Science and Technology Innovation Project of Laoshan Laboratory (LSKJ202300401, LSKJ202202201). JL and LRL were supported by Office of Science, U.S. Department of Energy (DOE) Biological and Environmental Research as part of the Regional and Global Model Analysis program area. Pacific Northwest National Laboratory is operated for DOE by Battelle Memorial Institute under contract DE-AC05-76RL01830.

References

Alizadeh, O. (2022). A review of the El Niño-Southern Oscillation in future. *Earth-Science Reviews, 235*. doi:10.1016/j.earscirev.2022.104246

Anstey, J. A., et al. (2013). Multi-model analysis of Northern Hemisphere winter blocking: Model biases and the role of resolution. *Journal of Geophysical Research-Atmospheres, 118*(10), 3956-3971. doi:10.1002/jgrd.50231

Athanasiadis, P. J., et al. (2022). Mitigating Climate Biases in the Midlatitude North Atlantic by Increasing Model Resolution: SST Gradients and Their Relation to Blocking and the Jet. *Journal of Climate, 35*(21), 6985-7006. doi:10.1175/jcli-d-21-0515.1

Barriopedro, D., & Calvo, N. (2014). On the Relationship between ENSO, Stratospheric Sudden Warmings, and Blocking. *Journal of Climate, 27*(12), 4704-4720. doi:https://doi.org/10.1175/JCLI-D-13-00770.1

Barriopedro, D., et al. (2011). The Hot Summer of 2010: Redrawing the Temperature Record Map of Europe. *Science, 332*(6026), 220-224. doi:10.1126/science.1201224

Barriopedro, D., et al. (2006). A climatology of northern hemisphere blocking. *Journal of*

683 *Climate, 19*(6), 1042-1063. doi:10.1175/jcli3678.1
684 Berckmans, J., et al. (2013). Atmospheric blocking in a high resolution climate model:
685 influences of mean state, orography and eddy forcing. *Atmospheric Science Letters, 14*(1), 34-40.
686 doi:10.1002/asl2.412
687 Beverley, J. D., et al. (2024). Drivers of Changes to the ENSO–Europe Teleconnection Under
688 Future Warming. *Geophysical Research Letters, 51*(10), e2023GL107957.
689 doi:https://doi.org/10.1029/2023GL107957
690 Cai, W., et al. (2021). Changing El Niño–Southern Oscillation in a warming climate. *Nature*
691 *Reviews Earth & Environment, 2*(9), 628-644. doi:10.1038/s43017-021-00199-z
692 Cattiaux, J., et al. (2010). Winter 2010 in Europe: A cold extreme in a warming climate.
693 *Geophysical Research Letters, 37*. doi:10.1029/2010gl044613
694 Davini, P., et al. (2012). Bidimensional Diagnostics, Variability, and Trends of Northern
695 Hemisphere Blocking. *Journal of Climate, 25*(19), 6496-6509. doi:10.1175/jcli-d-12-00032.1
696 Davini, P., & Cagnazzo, C. (2014). On the misinterpretation of the North Atlantic Oscillation
697 in CMIP5 models. *Climate Dynamics, 43*(5-6), 1497-1511. doi:10.1007/s00382-013-1970-y
698 Davini, P., & D'Andrea, F. (2016). Northern Hemisphere Atmospheric Blocking
699 Representation in Global Climate Models: Twenty Years of Improvements? *Journal of Climate,*
700 *29*(24), 8823-8840. doi:10.1175/jcli-d-16-0242.1
701 Davini, P., & D'Andrea, F. (2020). From CMIP3 to CMIP6: Northern Hemisphere
702 Atmospheric Blocking Simulation in Present and Future Climate. *Journal of Climate, 33*(23),
703 10021-10038. doi:10.1175/jcli-d-19-0862.1
704 De Luca, P., et al. (2024). Enhanced Blocking Frequencies in Very-High Resolution Idealized
705 Climate Model Simulations. *Geophysical Research Letters, 51*(22), e2024GL111016.
706 doi:https://doi.org/10.1029/2024GL111016
707 de Vries, H., et al. (2013). Atmospheric blocking and its relation to jet changes in a future
708 climate. *Climate Dynamics, 41*(9-10), 2643-2654. doi:10.1007/s00382-013-1699-7
709 Dong, L., et al. (2018). The Dynamical Linkage of Atmospheric Blocking to Drought,
710 Heatwave and Urban Heat Island in Southeastern US: A Multi-Scale Case Study. *Atmosphere,*
711 *9*(1). doi:10.3390/atmos9010033
712 Drouard, M., & Woollings, T. (2018). Contrasting Mechanisms of Summer Blocking Over
713 Western Eurasia. *Geophysical Research Letters, 45*(21), 12040-12048.
714 doi:10.1029/2018gl079894
715 Dunn-Sigouin, E., & Son, S.-W. (2013). Northern Hemisphere blocking frequency and
716 duration in the CMIP5 models. *Journal of Geophysical Research: Atmospheres, 118*(3), 1179-
717 1188. doi:10.1002/jgrd.50143
718 Eyring, V., et al. (2016). Overview of the Coupled Model Intercomparison Project Phase 6
719 (CMIP6) experimental design and organization. *Geoscientific Model Development, 9*(5), 1937-
720 1958. doi:10.5194/gmd-9-1937-2016
721 Fereday, D. R., et al. (2020). Tropical Rainfall Linked to Stronger Future ENSO-NAO
722 Teleconnection in CMIP5 Models. *Geophysical Research Letters, 47*(22), e2020GL088664.
723 doi:https://doi.org/10.1029/2020GL088664
724 Garrido-Perez, J. M., et al. (2018). Air stagnation in Europe: Spatiotemporal variability and

impact on air quality. *Sci Total Environ, 645*, 1238-1252. doi:10.1016/j.scitotenv.2018.07.238

Heukamp, F. O., et al. (2023). Cyclones modulate the control of the North Atlantic Oscillation on transports into the Barents Sea. *Communications Earth & Environment, 4*(1). doi:10.1038/s43247-023-00985-1

Jiang, T., et al. (2019). Northern Hemisphere Blocking in similar to 25-km-Resolution E3SM v0.3 Atmosphere-Land Simulations. *Journal of Geophysical Research-Atmospheres, 124*(5), 2465-2482. doi:10.1029/2018jd028892

Kautz, L.-A., et al. (2022). Atmospheric blocking and weather extremes over the Euro-Atlantic sector – a review. *Weather and Climate Dynamics, 3*(1), 305-336. doi:10.5194/wcd-3-305-2022

Kwon, Y.-O., et al. (2020). Impact of Multidecadal Variability in Atlantic SST on Winter Atmospheric Blocking. *Journal of Climate, 33*(3), 867-892. doi:10.1175/jcli-d-19-0324.1

Lau, W. K. M., & Kim, K.-M. (2012). The 2010 Pakistan Flood and Russian Heat Wave: Teleconnection of Hydrometeorological Extremes. *Journal of Hydrometeorology, 13*(1), 392-403. doi:10.1175/jhm-d-11-016.1

Li, C., & Sun, J. (2015). Role of the Subtropical Westerly Jet Waveguide in a Southern China Heavy Rainstorm in December 2013. *Advances in Atmospheric Sciences, 32*(5), 601-612. doi:10.1007/s00376-014-4099-y

Liu, P., et al. (2018). Climatology of tracked persistent maxima of 500-hPa geopotential height. *Climate Dynamics, 51*(1-2), 701-717. doi:10.1007/s00382-017-3950-0

Maddison, J. W., et al. (2021). Linking air stagnation in Europe with the synoptic- to large-scale atmospheric circulation. *Weather Clim. Dynam., 2*(3), 675-694. doi:10.5194/wcd-2-675-2021

Masato, G., et al. (2013). Winter and Summer Northern Hemisphere Blocking in CMIP5 Models. *Journal of Climate, 26*(18), 7044-7059. doi:10.1175/jcli-d-12-00466.1

Matsueda, M. (2009). Blocking Predictability in Operational Medium-Range Ensemble Forecasts. *Sola, 5*, 113-116. doi:10.2151/sola.2009-029

Matsueda, M., & Endo, H. (2017). The robustness of future changes in Northern Hemisphere blocking: A large ensemble projection with multiple sea surface temperature patterns. *Geophysical Research Letters, 44*(10), 5158-5166. doi:10.1002/2017gl073336

Matsueda, M., et al. (2009). Future change in wintertime atmospheric blocking simulated using a 20-km-mesh atmospheric global circulation model. *Journal of Geophysical Research-Atmospheres, 114*. doi:10.1029/2009jd011919

McKenna, M., & Karamperidou, C. (2023). The Impacts of El Niño Diversity on Northern Hemisphere Atmospheric Blocking. *Geophysical Research Letters, 50*(13). doi:10.1029/2023gl104284

Müller, W. A., & Roeckner, E. (2008). ENSO teleconnections in projections of future climate in ECHAM5/MPI-OM. *Climate Dynamics, 31*(5), 533-549. doi:10.1007/s00382-007-0357-3

Neal, E., et al. (2022). The 2021 Pacific Northwest Heat Wave and Associated Blocking: Meteorology and the Role of an Upstream Cyclone as a Diabatic Source of Wave Activity. *Geophysical Research Letters, 49*(8). doi:10.1029/2021gl097699

Nie, Y., et al. (2019). Winter and Summer Rossby Wave Sources in the CMIP5 Models. *Earth*

and Space Science, 6(10), 1831-1846. doi:10.1029/2019ea000674

Pelly, J. L., & Hoskins, B. J. (2003). A new perspective on blocking. *Journal of the Atmospheric Sciences, 60*(5), 743-755. doi:10.1175/1520-0469(2003)060<0743:Anpob>2.0.Co;2

Perkins-Kirkpatrick, S., et al. (2024). Extreme terrestrial heat in 2023. *Nature Reviews Earth & Environment, 5*(4), 244-246. doi:10.1038/s43017-024-00536-y

Pfahl, S. (2014). Characterising the relationship between weather extremes in Europe and synoptic circulation features. *Natural Hazards and Earth System Sciences, 14*(6), 1461-1475. doi:10.5194/nhess-14-1461-2014

Rayner, N. A., et al. (2003). Global analyses of sea surface temperature, sea ice, and night marine air temperature since the late nineteenth century. *Journal of Geophysical Research-Atmospheres, 108*(D14). doi:10.1029/2002jd002670

Rex, D. F. (1950a). Blocking Action in the Middle Troposphere and its Effect upon Regional Climate. *Tellus, 2*(4), 275-301. doi:10.1111/j.2153-3490.1950.tb00339.x

Rex, D. F. (1950b). Blocking Action in the Middle Troposphere and its Effect upon Regional Climate. *Tellus, 2*(3), 196-211. doi:10.1111/j.2153-3490.1950.tb00331.x

Scaife, A. A., et al. (2011). Improved Atlantic winter blocking in a climate model. *Geophysical Research Letters, 38*. doi:10.1029/2011gl049573

Scaife, A. A., et al. (2010). Atmospheric Blocking and Mean Biases in Climate Models. *Journal of Climate, 23*(23), 6143-6152. doi:10.1175/2010jcli3728.1

Schemm, S., et al. (2022). Storm track response to uniform global warming downstream of an idealized sea surface temperature front. *Weather Clim. Dynam., 3*(2), 601-623. doi:10.5194/wcd-3-601-2022

Schiemann, R., et al. (2020). Northern Hemisphere blocking simulation in current climate models: evaluating progress from the Climate Model Intercomparison Project Phase 5 to 6 and sensitivity to resolution. *Weather Clim. Dynam., 1*(1), 277-292. doi:10.5194/wcd-1-277-2020

Schiemann, R., et al. (2017). The Resolution Sensitivity of Northern Hemisphere Blocking in Four 25-km Atmospheric Global Circulation Models. *Journal of Climate, 30*(1), 337-358. doi:10.1175/jcli-d-16-0100.1

Schneidereit, A., et al. (2012). Large-Scale Flow and the Long-Lasting Blocking High over Russia: Summer 2010. *Monthly Weather Review, 140*(9), 2967-2981. doi:10.1175/mwr-d-11-00249.1

Schwierz, C., et al. (2004). Perspicacious indicators of atmospheric blocking. *Geophysical Research Letters, 31*(6). doi:10.1029/2003gl019341

Shaw, T. A., et al. (2024). Emerging Climate Change Signals in Atmospheric Circulation. *AGU Advances, 5*(6), e2024AV001297. doi:https://doi.org/10.1029/2024AV001297

Simpson, I. R., et al. (2020). An Evaluation of the Large-Scale Atmospheric Circulation and Its Variability in CESM2 and Other CMIP Models. *Journal of Geophysical Research-Atmospheres, 125*(13). doi:10.1029/2020jd032835

Small, R. J., et al. (2014). Storm track response to ocean fronts in a global high-resolution climate model. *Climate Dynamics, 43*(3), 805-828. doi:10.1007/s00382-013-1980-9

Steinfeld, D., & Pfahl, S. (2019). The role of latent heating in atmospheric blocking dynamics: a global climatology. *Climate Dynamics, 53*(9), 6159-6180. doi:10.1007/s00382-019-04919-6

Suitters, C. C., et al. (2023). Transient anticyclonic eddies and their relationship to atmospheric block persistence. *Weather Clim. Dynam., 4*(3), 683-700. doi:10.5194/wcd-4-683-2023

Sun, W., et al. (2019). How waviness in the circulation changes surface ozone: a viewpoint using local finite-amplitude wave activity. *Atmospheric Chemistry and Physics, 19*(20), 12917-12933. doi:10.5194/acp-19-12917-2019

Tibaldi, S., et al. (1997). Climatology of Northern Hemisphere blocking in the ECHAM model. *Climate Dynamics, 13*(9), 649-666. doi:10.1007/s003820050188

Williams, N. C., et al. (2024). Effect of increased ocean resolution on model errors in El Niño–Southern Oscillation and its teleconnections. *Quarterly Journal of the Royal Meteorological Society, 150*(760), 1489-1500. doi:https://doi.org/10.1002/qj.4655

Woollings, T., et al. (2018). Blocking and its Response to Climate Change. *Current climate change reports, 4*(3), 287-300. doi:10.1007/s40641-018-0108-z

Woollings, T., et al. (2014). Arctic warming, atmospheric blocking and cold European winters in CMIP5 models. *Environmental Research Letters, 9*(1). doi:10.1088/1748-9326/9/1/014002

Woollings, T., et al. (2008). A new Rossby wave-breaking interpretation of the North Atlantic Oscillation. *Journal of the Atmospheric Sciences, 65*(2), 609-626. doi:10.1175/2007jas2347.1

Xu, P., et al. (2020). The record-breaking heat wave of June 2019 in Central Europe. *Atmospheric Science Letters, 21*(4). doi:10.1002/asl.964

Yao, Y., et al. (2023). Extreme Cold Events in North America and Eurasia in November-December 2022: A Potential Vorticity Gradient Perspective. *Advances in Atmospheric Sciences, 40*(6), 953-962. doi:10.1007/s00376-023-2384-3

Zhang, R. N., et al. (2018). The impact of Arctic sea ice on the inter-annual variations of summer Ural blocking. *International Journal of Climatology, 38*(12), 4632-4650. doi:10.1002/joc.5731